Magnetorotational instability of dissipative Couette flow

By JEREMY GOODMAN[1] AND HANTAO JI[2]

[1]Princeton University Observatory, Princeton, NJ 08544, USA

[2]Princeton Plasma Physics Laboratory, Princeton University, P.O. Box 451, Princeton, NJ 08543, USA

Axisymmetric stability of viscous resistive magnetized Couette flow is re-examined, with the emphasis on flows that would be hydrodynamically stable according to Rayleigh's criterion: opposing gradients of angular velocity and specific angular momentum. In this regime, magnetorotational instabilities (MRI) may occur. Previous work has focused on the Rayleigh-unstable regime. To prepare for an experimental study of MRI, which is of intense astrophysical interest, we solve for global linear modes in a wide gap with realistic dissipation coefficients. Exchange of stability appears to occur through marginal modes. Velocity eigenfunctions of marginal modes are nearly singular at conducting boundaries, but magnetic eigenfunctions are smooth and obey a fourth-order differential equation in the inviscid limit. The viscous marginal system is of tenth order; an eighth-order approximation previously used for Rayleigh-unstable modes does not permit MRI. Peak growth rates are insensitive to boundary conditions. They are predicted with surprising accuracy by WKB methods even for the largest-scale mode. We conclude that MRI is achievable under plausible experimental conditions using easy-to-handle liquid metals such as gallium.

1. Introduction

To an even greater extent than large-scale terrestrial flows, astrophysical flows are nearly inviscid. Yet observations show that they dissipate efficiently. For example, accretion disks (flattened systems of gas in orbit about a star or black hole) must lose orbital energy in order that the gas flow onto the central object. Shear-driven turbulence has long been implicated, but purely hydrodynamic turbulence is probably ineffective because of the strongly stable radial angular momentum gradient in the disk. When warm enough to be partially ionized, as they often are, accretion disks become magnetohydrodynamic (MHD) fluids. It is now believed that turbulence and orbital decay are driven by magnetorotational instabilities (MRI).

Although discovered by Velikhov (1959) and Chandrasekhar (1960), MRI did not come to the attention of the astrophysical community until rediscovered by Balbus & Hawley (1991). MRI requires that the angular velocity decrease with distance from the rotation axis, $\partial \Omega^2/\partial r < 0$. Unlike Rayleigh's centrifugal instability, MRI may occur when specific angular momentum increases with radius, $\partial (r^2 \Omega)^2/\partial r > 0$. These conditions arise in accretion disks, where the angular velocity $\Omega \propto r^{-3/2}$. Simple axisymmetric instability occurs if the magnetic field is purely axial. In ideal MHD, the maximum growth rate is independent of the field strength; however, the wavelength

of fastest growth is then proportional to the field, so that a resistive fluid has a minimum field strength for instability. When the background field has azimuthal as well as axial components, MRI modes are overstable and the growth rate is reduced (Knobloch 1992); however, it is difficult to stabilize a disk completely if there is any axial field (Gammie & Balbus 1994; Curry & Pudritz 1995). Purely azimuthal field does not have *local* MRI instabilities, but non-axisymmetric disturbances can be very strongly, though transiently, amplified (Balbus & Hawley 1992; Terquem & Papaloizou 1996), and global non-axisymmetric instabilities arise with suitable radial boundaries (Ogilvie & Pringle 1996). It is not clear whether radially local or global analyses of idealized incompressible systems are more relevant to accretion disks, because disks tend to be very thin in the axial direction compared to their radial extent, and because the horizontal shear is supersonic on all scales larger than the thickness.

Many nonlinear computer simulations of MRI have been performed. Most of the well-resolved simulations have been made in a local Cartesian geometry intended to represent a small portion of a disk, with artificial boundary conditions. Where comparison is possible, local results are consistent with global simulations (Stone & Norman 1994; Matsumoto *et al.* 1996; Armitage 1998; Machida, Hayashi & Matsumoto 2000; Hawley, Balbus & Stone 2001; Hawley 2001; Hawley & Krolik 2001; Art & Rüdiger 2001). Among the more important and generally accepted results are the following (see Balbus & Hawley 1998, for a review and references up to 1997). Starting from equilibrium conditions, instability develops as predicted by local linear theory. When constrained to be axisymmetric, the nonlinear outcome is an extension of the linear mode, apart from effects of compressibility (most simulations assume a compressible fluid); but three-dimensional simulations tend to become fully turbulent. Sustained turbulence is strongest when the axial field has a non-zero spatial average over the disk or local computational volume, i.e. $\langle B_z \rangle \neq 0$ (Hawley, Gammie & Balbus 1996). Even when $\langle B_z \rangle = 0$, however, the field energy and turbulence apparently sustain themselves indefinitely in the presence of a steady mean shear, provided that resistive effects are sufficiently weak (Brandenburg *et al.* 1995; Hawley, Gammie & Balbus 1995; Fleming, Stone & Hawley 2000).

There exists a body of experimental work on magnetized Couette flow (Donnelly & Ozima 1960, 1962; Donnelly & Caldwell 1964; Brahme 1970), but the MRI has never been demonstrated in the laboratory. The main obstacle is that liquid metals are strongly resistive on laboratory scales, with magnetic diffusivity $\eta \gtrsim 10^3\,\mathrm{cm^2\,s^{-1}}$. The viscosity is much smaller, typically $v \sim 10^{-3}\,\mathrm{cm^2\,s^{-1}}$. Their ratio is the magnetic Prandtl number $P_m \equiv v/\eta \sim 10^{-6}$.

Chandrasekhar (1961) also analysed *dissipative* magnetized Couette flow. After laying out general equations for viscous and resistive linearized axisymmetric perturbations, he discarded a term involving shear from the azimuthal induction equation on the grounds that $P_m \ll 1$. In fact the neglected term involves neither v nor η directly. Thus the commonly used name 'small-P_m approximation' is somewhat unfortunate. It presumes that viscous and inertial forces are comparable throughout the flow. Although this is often the case for marginal Rayleigh instabilities resisted by viscous (and perhaps magnetic) forces, it is not the case for the MRI modes of interest here, where viscosity is important in boundary layers only. We shall show that MRI modes do not exist in Chandrasekhar's approximation (§ 3). (Of course he did find MRI modes, but in a separate analysis assuming ideal MHD.) We shall introduce a different $P_m \to 0$ limit that retains all terms in the induction equation but neglects viscous boundary layers.

Chandrasekhar's results have been refined by Chang & Sartory (1967), Hassard, Chang & Ludford (1972), Vislovich, Novikov & Sinitsyn (1986), Takhar, Ali & Soundalgekar (1989), Soundalgekar, Ali & Takhar (1994) and Chen & Chang (1998), but always under Chandrasekhar's 'small-P_m' approximation.

In a previous paper (Ji, Goodman & Kageyama 2001, henceforth referred to as Paper I), we have used local WKB methods to survey the MRI regime for realistic materials and laboratory parameters. The most unstable modes (and perhaps the only ones accessible to experiment in the near term) have wavelengths twice as large as the apparatus, so that WKB methods are not to be trusted *a priori*. The present paper therefore discusses the global linear analysis. We integrate the full set of viscous and resistive equations via an initial-value scheme to obtain numerical growth rates for cases that would be stable by Rayleigh's criterion. The locally obtained growth rates are found to be good approximations, even though the radial eigenfunctions are far from being sinusoidal. We predict instability under feasible conditions: gap widths and heights of order 10 cm, field strengths of several kiloGauss, and rotation rates of several hundred radians per second.

A supplementary analysis shows that curves of marginal MRI stability are well-approximated by completely neglecting viscous terms, especially for insulating cylinders. Although $P_m \to 0$, this is not Chandrasekhar's approximation. It eliminates the velocity perturbations from the analysis and leads to a system of only four radial derivatives. The boundary conditions on velocity are not satisfied by the reduced system even with stress-free (slipping) boundaries. This is resolved by restoring the viscosity, as we show by a boundary analysis (§4) and by numerical examples (§5). The magnetic eigenfunctions and the growth rate are insensitive to the viscosity when P_m is small. When characterizing stability of MRI modes in liquid metals, dimensionless numbers based on viscosity, such as the Hartmann and Taylor numbers, are less natural than numbers that remain finite as $P_m \to 0$, such as the Lundquist number and magnetic Reynolds number.

2. Basic equations and boundary conditions

We use cylindrical coordinates r, θ, z aligned with the rotation of the fluid, and Gaussian electromagnetic units. In equilibrium, the magnetic field is constant and parallel to the axis; it is described by the associated Alfvén speed $V_A \equiv B_0/(4\pi\rho)^{1/2}$, where ρ is the (constant) density of the liquid metal. (In ideal MHD, a uniformly magnetized incompressible fluid supports transverse waves that propagate along field lines at speed V_A. The angular velocity is $\Omega(r)$; see e.g. Roberts (1967).) Perturbations are axisymmetric and sinusoidal in z with wavelength $2\pi/k$:

$$\left.\begin{aligned}
\delta B_r/(4\pi\rho)^{1/2} &= \beta_r(r,t)\cos kz, & \delta v_r &= \varphi_r(r,t)\sin kz, \\
\delta B_\theta/(4\pi\rho)^{1/2} &= \beta_\theta(r,t)\cos kz, & \delta v_\theta &= \varphi_\theta(r,t)\sin kz, \\
\delta B_z/(4\pi\rho)^{1/2} &= \beta_z(r,t)\sin kz, & \delta v_z &= \varphi_z(r,t)\cos kz.
\end{aligned}\right\} \qquad (2.1)$$

We often write $h \equiv \pi/k$ for half the wavelength, having in mind an experiment of finite height h and rigid vertical boundaries.

Perturbations associated with a single mode are exponential in time, but it is convenient to allow for general time dependence and discover the fastest-growing mode by integrating the linearized equations forward in time. These equations are

(see the Appendix)

$$\dot{\beta}_\theta = \eta(D - k^2)\beta_\theta + kV_A\varphi_\theta + \underline{r\Omega'\beta_r}, \tag{2.2}$$

$$\dot{\varphi}_\theta = \nu(D - k^2)\varphi_\theta - kV_A\beta_\theta - r^{-1}(r^2\Omega)'\varphi_r, \tag{2.3}$$

$$\dot{\beta}_r = \eta(D - k^2)\beta_r + kV_A\varphi_r, \tag{2.4}$$

$$\dot{\varphi}_r = \nu(D - k^2)\varphi_r - kV_A\beta_r + \Pi, \tag{2.5}$$

$$(k^2 - D)\Pi = 2\Omega k^2\varphi_\theta. \tag{2.6}$$

The prime in equations (2.2) and (2.3) stands for $\partial/\partial r$, and

$$D \equiv \frac{\partial^2}{\partial r^2} + \frac{1}{r}\frac{\partial}{\partial r} - \frac{1}{r^2}.$$

Note that Chandrasekhar (1961) denotes the latter operator by DD_*.

Equations (2.2) and (2.3) are the azimuthal components of the induction and Euler equations, while (2.4) and (2.5) are the corresponding radial components. By eliminating the auxiliary function Π between equations (2.5) and (2.6), one obtains an equation equivalent to Chandrasekhar's equation (168), although some differences in sign occur because we have taken perturbations proportional to $\sin kz$ where he took $\cos kz$ and vice versa. Our equations (2.2), (2.3) and (2.4) correspond to his equations (163), (160) and (162), respectively.

The flow is confined between concentric cylinders with radii $r_1 < r_2$. If these are perfectly conducting, the magnetic boundary conditions are

$$\beta_r = 0, \qquad (r\beta_\theta)' = 0. \tag{2.7}$$

If perfectly insulating, then (I_n and K_n are modified Bessel functions)

$$\frac{\partial}{\partial r}(r\beta_r) = \beta_r \times \left\{ \begin{array}{ll} [krI_0(kr)]/I_1(kr) & \text{at} \quad r = r_1 \\ -[krK_0(kr)]/K_1(kr) & \text{at} \quad r = r_2, \end{array} \right\}$$
$$\beta_\theta = 0 \quad \text{at} \quad r = r_1, r_2. \tag{2.8}$$

The conditions on velocity are

$$\varphi_r = 0, \qquad \nu\varphi_\theta = 0 = \nu(r\varphi_r)'. \tag{2.9}$$

We have put the viscosity in the latter two conditions so that φ_θ and $\varphi_z = (r\varphi_r)'/(kr)$ will be unconstrained when the flow is inviscid.

The insulating condition (2.8) on β_r is not accurate for an experiment of finite height $h = \pi/k$, since it assumes a vertically periodic solution for the vacuum field outside the cylinders. The conducting conditions (2.7) do not have this drawback. In both cases, there will be viscous boundary layers at the top and bottom (unless the end caps rotate differentially), but we expect that the error caused by neglecting those layers is small for $P_m \sim 10^{-6}$ and growth times shorter than the Ekman circulation time. In any event, the end caps should be insulating so that no magnetic stress acts upon them.

3. Why the small-P_m approximation suppresses the MRI

The underlined term in equation (2.2) is the critical one that Chandrasekhar (1961) and subsequent authors discarded on the grounds that $P_m \ll 1$. To see that this term is necessary to the MRI, it is useful to reduce equations (2.2)–(2.6) to a single equation.

For brevity, assume a mode with definite growth rate s, and write $D_k \equiv D - k^2$,

$\omega_A \equiv kV_A$. Equation (2.4) yields

$$\varphi_r = \omega_A^{-1}(s - \eta \mathrm{D}_k)\beta_r. \tag{3.1}$$

Substituting for φ_r in equation (2.5), applying D_k, and eliminating $\mathrm{D}_k\Pi$ via equation (2.6), gives

$$\varphi_\theta = -(2\Omega k^2 \omega_A)^{-1}[(s - \nu\mathrm{D}_k)(s - \eta\mathrm{D}_k) + \omega_A^2]\mathrm{D}_k\beta_r. \tag{3.2}$$

Solving for β_θ from equation (2.3) and eliminating φ_θ and φ_r in favour of β_r, gives

$$\beta_\theta = \omega_A^{-2}\left\{(s - \nu\mathrm{D}_k)\frac{1}{2\Omega k^2}[(s - \nu\mathrm{D}_k)(s - \eta\mathrm{D}_k) + \omega_A^2]\mathrm{D}_k - \frac{(r^2\Omega)'}{r}(s - \eta\mathrm{D}_k)\right\}\beta_r. \tag{3.3}$$

Using these to eliminate φ_θ and β_θ from equation (2.2) yields the desired tenth-order equation:

$$\left\{[(s - \nu\mathrm{D}_k)(s - \eta\mathrm{D}_k) + \omega_A^2]\frac{1}{2\Omega}[(s - \nu\mathrm{D}_k)(s - \eta\mathrm{D}_k) + \omega_A^2](-k^{-2}\mathrm{D}_k)\right.$$
$$\left. + (s - \eta\mathrm{D}_k)\frac{(r^2\Omega)'}{r}(s - \eta\mathrm{D}_k)\right\}\beta_r = -\omega_A^2\underline{r\Omega'\beta_r}. \tag{3.4}$$

We are interested in Rayleigh-stable cases. Without loss of generality, we may assume that the angular velocity (Ω) and vorticity $(r^{-1}(r^2\Omega)')$ are positive throughout the flow, but the shear $(r\Omega')$ may be negative. Now D_k is clearly negative definite and self-adjoint with either of the boundary conditions (2.7) or (2.8). In the narrow-gap limit $(r_2 - r_1)/(r_2 + r_1) \to 0$, the angular velocity and vorticity are positive constants. It follows that the operator in braces in the left-hand side of equation (3.4) is positive definite for non-negative real s. Therefore, *at least in the narrow-gap limit, there can be no modes with positive real growth rate when the underlined shear term is neglected and the Rayleigh stability criterion is satisfied*. We interpret this to mean that the MRI is not present.

Previous studies of the time-dependent problem have discarded the time derivatives in the induction equation as well as the underlined term (Chang & Sartory 1967; Chen & Chang 1998); in this case, the operator in question becomes quadratic in s so that the coefficient of $\mathrm{Im}(s)$ is positive-definite for $\mathrm{Re}(s) > 0$, which rules out complex growing modes, i.e. overstabilities.

Unfortunately, we cannot draw such strong conclusions in the wide-gap case where Ω and perhaps also $r^{-1}(r^2\Omega)'$ vary significantly with radius. The operator on the left-hand side of equation (3.4) is no longer self-adjoint in general, because D_k and Ω do not commute. For marginal modes, however,

$$\left\{\left[\nu\mathrm{D}_k^2 + \frac{\omega_A^2}{\eta}\right]\frac{\eta}{2\Omega k^2}\left[\nu\mathrm{D}_k^2 + \frac{\omega_A^2}{\eta}\right] - \eta\mathrm{D}_k\frac{(r^2\Omega)'}{r}\right\}\varphi_r = -\omega_A\underline{r\Omega'\beta_r}, \tag{3.5}$$

in which we have used equation (3.1). In this case the problem is only eighth order in radial derivatives if the right-hand side is neglected, as noted by Chandrasekhar (1961). More importantly, the operator in these curly braces is self-adjoint in the interesting special case that

$$\Omega(r) = a + \frac{b}{r^2}, \tag{3.6}$$

since $r^{-1}(r^2\Omega)' = 2a$ is then constant, and the rest of the operator is symmetrical. Equation (3.6) is the angular-velocity profile of a Couette flow in steady state, because it implies a radially constant viscous angular-momentum flux. We conclude that there

are no Rayleigh-stable *marginal* modes when the magnetic shear term is neglected, even for wide gaps.

4. Boundary-layer analysis for marginal modes

If $v = 0$, then as the growth rate $s \to 0$, equation (3.4) reduces to

$$\left[\eta^2 D_k \frac{(r^2\Omega)'}{r} - \frac{\omega_A^4}{2\Omega k^2} \right] D_k \beta_r = -\omega_A^2 r\Omega' \underline{\beta_r}. \tag{4.1}$$

Even with the right-hand side included, this is only a fourth-order system. Paradoxically, there are six boundary conditions to be satisfied: φ_θ and φ_z are not constrained when $v = 0$, but $\varphi_r = 0$ at both boundaries, in addition to a total of four magnetic conditions. For the insulating case (2.8), the paradox is resolved because equations (3.1) and (3.3) show that both $\varphi_r = 0$ and $\beta_\theta = 0$ are equivalent to $D_k \beta_r = 0$, so that there are only four independent boundary conditions after all. But in the conducting case (2.7), we have via equations (3.1)–(3.3) that $\beta_r = D_k \beta_r = (r D_k \beta_r)' = 0$ at both boundaries, and not all six conditions can be satisfied.

The crux of the difficulty is the azimuthal Euler equation (2.3), which reduces to an algebraic relation. At zero viscosity and growth rate, azimuthal force balance requires

$$2\Omega \delta v_r = \frac{B_0}{4\pi\rho} \frac{\partial \delta B_\theta}{\partial z}, \tag{4.2}$$

so that the Lorentz force ($\delta j_r \times B_0$) balances the Coriolis force, which vanishes at the boundary. If the boundary is insulating, then δB_θ ($\propto \delta j_r$) also vanishes. But at conducting boundaries, $\delta B_\theta \neq 0$ ($\delta j_r \neq 0$), so that viscosity must intervene to maintain the azimuthal force balance. For small P_m, the marginal eigenfunction displays a dramatic boundary layer (figure 3).

Viscous boundary layers are common in hydrodynamics. Normally they occur because the tangential component of velocity must match that of the boundary itself, even when the viscosity is small (a 'no-slip' boundary condition). For conducting cylinders, however, a boundary layer would occur even if the viscous stress vanished at the boundary, because of the impossibility of satisfying equation (4.2). In the present case, the viscous layer is driven by tangential magnetic field (or normal component of current) rather than tangential velocity.

To clarify the relationship between the viscous and inviscid problems, especially when $s = 0$, we now perform a boundary-layer analysis. Our problem differs from a standard Hartmann layer (e.g. Roberts 1967) because of the importance of Coriolis forces; and also because, when the cylinders are conducting, there is no component of the field perpendicular to the boundary.

Since the viscosity is small, we let δ be the characteristic width of the boundary layer and suppose that $\delta \propto v^n$ is small compared to the cylinder height and gap width; the scaling exponent n is positive but as yet undetermined. For definiteness, we restrict the discussion to the inner boundary $r \approx r_1$. Let $x = (r - r_1)/\delta$ be a dimensionless coordinate perpendicular to this boundary. On the scale δ, background quantities such as Ω, $r\Omega'$, $r^{-1}(r^2\Omega)'$ and r itself can be regarded as constants. Hence (3.4) is an equation in constant coefficients, so that the quantities (2.1) vary with x as a superposition of fundamental solutions having exponential dependence:

$$(\beta_r, \dots, \phi_z) \approx e^{st} \sum_{\alpha=1}^{10} \mathbf{y}^{(\alpha)} \exp(q_\alpha x),$$

the amplitudes $\boldsymbol{y}^{(\alpha)} = (\beta_r^{(\alpha)}, \ldots, \phi_z^{(\alpha)})$ being constant. The dimensionless wavenumbers $\{q_\alpha\}$ are the roots of the equation obtained by substituting $\beta_r \propto \exp(qx)$ into (3.4):

$$q^{10} + \left(\frac{2\omega_A^2 \delta^4}{\nu\eta}\right) q^6 - \left(\frac{\kappa^2 k^2 \delta^6}{\nu^2}\right) q^4 + \left(\frac{\omega_A^4 \delta^8}{(\nu\eta)^2}\right) q^2 + (4\Omega^2 - \kappa^2) \left(\frac{\omega_A^2 k^2 \delta^{10}}{(\nu\eta)^2}\right) = 0. \quad (4.3)$$

We have introduced the epicyclic frequency κ,

$$\kappa^2 \equiv \frac{1}{r^3} \frac{\mathrm{d}}{\mathrm{d}r}(r^2\Omega)^2. \quad (4.4)$$

One sees that (4.3) will be well-behaved in the limit $\nu \to 0$ if $\delta \propto \nu^{1/3}$. Therefore, we choose

$$\delta = \left(\frac{\nu}{\kappa k}\right)^{1/3}, \quad (4.5)$$

so that the coefficient of q^4 is (-1). This is not the Hartmann-layer thickness $\delta_H = (\eta\nu)^{1/2}/V_A$. Instead, $\delta \approx h^{1/3}\delta_E^{2/3}$, where $\delta_E = (2\nu/\kappa)^{1/2}$ is the thickness of the Ekman-layer and $h = \pi/k$ is the cylinder height. The coefficients of q^6, q^2 and q^0 in (4.3) are much smaller than unity provided that $\mu \ll 1$, where

$$\mu \equiv \frac{\omega_A^2 \nu^{1/3}}{\eta(k\kappa)^{4/3}} = \frac{\omega_A^2}{\eta k^2 \kappa} k\delta. \quad (4.6)$$

Clearly, $\mu \to 0$ as $\nu \to 0$ for any $\kappa \neq 0$. But the inviscid limit is approached rather slowly because of the cube root in (4.5). In terms of the local values of the Lundquist number S (equation (5.5)), magnetic Reynolds number R_m (equation (5.6)), fluid Reynolds number $Re = R_m/P_m$, and vorticity parameter ζ (equation (5.7)), one has the scalings $k\delta \approx \zeta^{-1/6}(Re)^{-1/3}$, and $\mu/k\delta \approx \zeta^{-1/2}S^2/R_m$ for modes whose vertical wavelength π/k is comparable to the gap width. For the experimental regime discussed below, $P_m \sim O(10^{-6})$, $S \sim R_m \sim O(1)$, and $\zeta \sim O(10^{-2})$ at the inner boundary, so that $k\delta \sim O(10^{-2})$ and $\mu \sim O(10^{-1})$.

We rewrite (4.3) as

$$q^{10} + 2\mu q^6 - q^4 + \mu^2 q^2 + \mu^4 F = 0, \quad (4.7)$$

where $F \equiv \kappa^2(4\Omega^2 - \kappa^2)(\eta k^2)^2/\omega_A^6$ is independent of viscosity and $\sim O(1)$. Then in the limit $\mu \to 0$, $q^4(q^6 - 1) = 0$, so that the non-zero $\{q_\alpha\}$ are the 6 sixth roots of unity. We shall call the corresponding $\boldsymbol{y}^{(\alpha)}$ 'microscopic' because they vary on scales $\sim O(\delta)$. Exactly half of them increase exponentially away from the boundary, while the other half decrease. Clearly the amplitudes of the former must be set to zero in order to match onto a smooth flow in the interior, while the amplitudes of the other three microscopic solutions can be adjusted to satisfy boundary conditions.

The remaining four roots for q in (4.7) approximately satisfy the reduced equation $q^4 - \mu^2 q^2 + \mu^4 F \approx 0$, so that $q \sim O(\mu)$; this implies a radial lengthscale that is $O(\delta/\mu)$ and therefore macroscopic: that is, independent of ν as $\nu \to 0$. Any superposition of the corresponding four $\boldsymbol{y}^{(\alpha)}$ might match onto a smooth interior flow. Hence there are a total of $7 = (3$ microscopic$) + (4$ macroscopic$)$ adjustable parameters to meet the $5 = (3$ no-slip$) + (2$ magnetic$)$ boundary conditions given by (2.9) and (2.7) or (2.8).

This leaves two parameters at each boundary that are not locally determined, but follow from the full solution for the linearized flow across the gap between cylinders. The fourth-order inviscid equation (4.1), together with the magnetic boundary conditions (2.7) or (2.8), has the same number of locally undetermined parameters at each

boundary. Thus one can see in general terms how the tenth-order system (2.2)–(2.6) reduces to the fourth-order equation (4.1) in the inviscid, marginal limit.

In more detail, one can solve the boundary-layer problem for marginal modes to leading order in $k\delta$ and μ in two steps as follows. First, solve (4.1) with the magnetic conditions (2.8) or (2.7) to obtain the magnetic variables throughout the gap. In general, the velocities derived from this solution via (3.1), (3.2) do not satisfy the boundary conditions (2.9); even the radial velocity may be non-zero when boundaries are conducting, as discussed following (4.2). In the second step, adjust the amplitudes of the three permissible microscopic boundary-layer functions (i.e. those that decay with distance from the wall) in order to satisfy the velocity boundary conditions. These adjustments have no effect on the magnetic boundary conditions to leading order because the magnetic components of the microscopic solutions are smaller than their velocity components by $O(v)$ or $O(v^{2/3})$, as can be verified from (3.1) and (3.2).

We have assumed $\mu \ll 1$, as appropriate for $v \to 0$ and for the experiments envisaged in §5. Let us briefly consider the alternative case that $\mu \gg 1$, as may occur if the magnetic field is sufficiently strong or the angular-momentum gradient $\kappa^2 \to 0$. The coefficient of q^6 in (4.3) is now larger than that of q^4, so instead of (4.5), we choose the boundary-layer lengthscale as

$$\delta' \equiv (v\eta/\omega_A^2)^{1/4},$$

using a prime to distinguish this from the earlier choice (4.5); then $\delta' \approx (h\delta_H)^{1/2}$, and

$$(k\delta')^{-2} = \frac{\omega_A}{k^2\sqrt{v\eta}} \equiv Q$$

is a Hartmann number, which we suppose to be large. In place of (4.7) we have

$$q^{10} + 2q^6 - \mu^{-3/2}q^4 + q^2 + \frac{4\Omega^2 - \kappa^2}{\omega_A^2 Q} = 0.$$

There are then 8 microscopic roots, determined approximately by $(q^4 + 1)^2 = 0$, of which half are well-behaved, i.e. decay with distance from the boundary, and two macroscopic roots, with physical scale lengths $\delta'/q \approx \pm(4\Omega^2 - \kappa^2)^{1/2}/V_A$. This leaves only $4 + 2 - 5 = 1$ locally undetermined degree of freedom, fewer by one than when $\mu \ll 1$, so the boundary is more influential for the interior flow.

The considerations of this section are important mainly in order to demonstrate that marginal modes are possible, i.e. that they are not incompatible with the boundary conditions required of the Couette flow. By inspection of (3.4), one can see that the boundary layer is likely to be significantly modified if the growth rate $s \gtrsim v/\delta^2$, or equivalently in view of (4.5), $s \gtrsim \kappa k\delta$.

5. Numerical results

We have approximated (2.2)–(2.6) by finite-difference equations on a radial grid uniformly spaced in $x \equiv \ln r$. The background angular velocity has the form (3.6), since this is easiest to realize experimentally. It is possible and convenient to resolve the boundary layers directly when they occur, so that a single numerical method can be used for both growing and marginal modes. According to the discussion in §4, the minimum number of grid cells (N) required to resolve the boundary layers of marginal modes is $\sim P_m^{-1/3} \sim 10^2$; since the calculations are not expensive, we use $N \geqslant 10^3$. Our scheme has second-order spatial accuracy, even at the boundaries. To
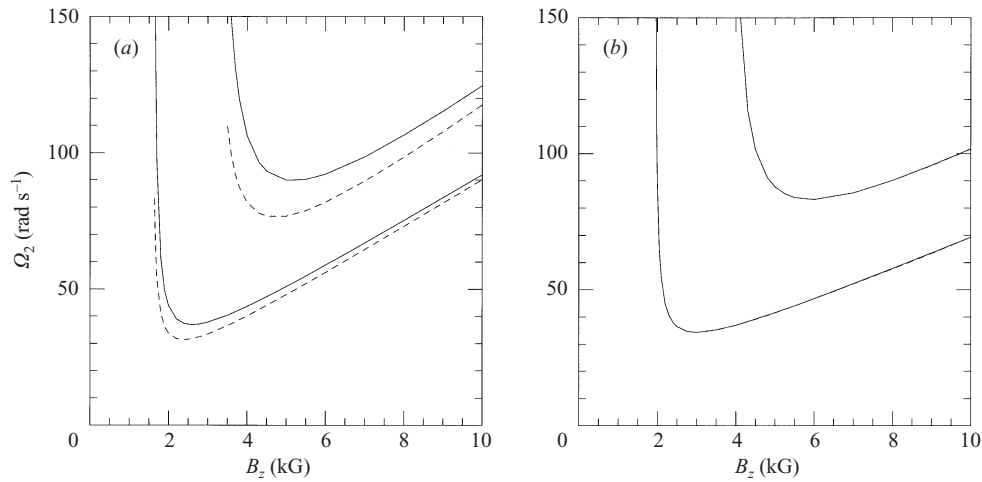
FIGURE 1. (*a*) Marginal stability for liquid gallium Couette flow between conducting cylinders of radii $r_1 = 5$ cm, $r_2 = 15$ cm, and height $h = 10$ cm. Solid lines are computed from equations (2.2)–(2.6); dashed from inviscid approximation (5.9) and (5.10). Lower curves are for mean dimensionless vorticity $\bar{\zeta} = 0.0632$ (corresponding to $\zeta(r_2) = 2/11$), upper ones for $\bar{\zeta} = 0.2205$ ($\zeta(r_2) = 4/7$). Instability occurs above the curves. In dimensionless parameters, $S \approx 0.92(B/10\,kG)$; and $\bar{R}_m \approx 0.66(\Omega_2/100\,\text{rad s}^{-1})$ (upper curves), $\bar{R}_m \approx 0.73(\Omega_2/100\,\text{rad s}^{-1})$ (lower). (*b*) As (*a*) but for insulating cylinders (2.8). Viscous and inviscid results differ by less than the line thickness.

ensure numerical stability, we use fully implicit time differencing. Spatial differences are written in terms of the unknown dependent variables at the new time step, so that a large linear system must be solved. Actually, our finite-difference matrix is band diagonal with 10 non-zero codiagonals in each of $5N$ rows, and it is independent of time step. We perform *LU* decomposition at the start of the evolution so that only the back substitution must be performed anew at each step.

When a growing mode is present, it eventually dominates. Then the perturbation in the radial magnetic field at successive time steps t_n and $t_{n+1} = t_n + \Delta t$ are related by, for example,

$$(1 - \hat{s}\Delta t)\hat{\beta}_r(x_j, t_{j+1}) = \hat{\beta}_r(x_j, t_j), \tag{5.1}$$

if $\hat{s} > 0$ is the appropriate eigenvalue of the matrix defined by the spatial difference scheme and therefore an estimate of the physical growth rate, and $\hat{\beta}_r$ is the corresponding eigenvector. Given $\hat{\beta}_r(x_j, t_j)$ and $\hat{\beta}_r(x_j, t_{j+1})$, we can compute $\hat{s}$ from equation (5.1) without any truncation error in Δt as long as $\hat{s}\Delta t < 1$. The eigenfunctions are similarly independent of Δt. This is advantageous close to marginal stability where $\hat{s}$ is small. Our procedure is equivalent to finding the most-positive eigenvalue of the time-evolution matrix by inverse iteration. By extending equation (5.1) to a three-term recurrence relation, we have allowed for complex eigenvalues. But in practice, all of our growing modes appear to have purely real values of $\hat{s}$. Of course, our method is not immune to spatial truncation errors; these are $O(\Delta x^2)$ because we use second-order spatial differencing.

Our initial-value code can treat slightly stable cases as well as unstable ones. By interpolation, we find parameters for marginal stability. Results are shown in figures 1(*a*) and 1(*b*) for material properties approximating liquid gallium: $\rho = 6$ g cm^{-3}, $\eta = 2000$ cm^2 s^{-1} and $P_m = 1.6 \times 10^{-6}$.

Marginal stability defines one constraint among the eight parameters defining the

Couette flow: η, v, r_1, r_2, k, Ω_1, Ω_2 and V_A. Six independent dimensionless combinations of these can be formed. The magnetic Prandtl number $P_m \equiv v/\eta$ is one of these. The ratios

$$A \equiv \frac{r_2 + r_1}{d} \tag{5.2}$$

and

$$\epsilon \equiv \frac{h}{d} \tag{5.3}$$

define the geometry, where $d \equiv r_2 - r_1$ is the gap width and $h \equiv \pi/k$ is half the vertical wavelength. It turns out that the magnetic eigenfunctions β_r and β_θ of the most unstable mode have a roughly parabolic dependence on r, and since one or the other vanishes at both boundaries, the effective horizontal wavenumber is $\approx \pi/d$. The total wavenumber is then

$$K \equiv \left(k^2 + \frac{\pi^2}{d^2} \right)^{1/2} = \frac{\pi}{h} \sqrt{1 + \epsilon^2}. \tag{5.4}$$

The Lundquist number

$$S \equiv \frac{kV_A}{\eta K^2} = \frac{V_A h}{2\pi\eta} \frac{2}{\epsilon^2 + 1} \tag{5.5}$$

scales the Alfvén frequency in terms of the magnetic diffusion rate ηK^2. In astrophysics, S is often called 'magnetic Reynolds number'. The plasma community generally reserves the latter term for a quantity involving fluid velocity, so we define the local magnetic Reynolds number by

$$R_m(r) \equiv \frac{\Omega}{\eta K^2}. \tag{5.6}$$

The viscous Reynolds number is of course R_m/P_m. The dimensionless vorticity

$$\zeta(r) \equiv \frac{(r^2\Omega)'}{r\Omega} \tag{5.7}$$

parametrizes the angular momentum gradient, and the Rayleigh stability criterion is simply $\zeta(r) \geqslant 0$. In the astrophysical literature, the radial variation of angular velocity is often described by an index

$$q \equiv -\frac{\mathrm{d}\ln\Omega}{\mathrm{d}\ln r} \quad \text{so that} \quad \zeta = 2 - q.$$

Of course, $\zeta = 2$ and $q = 0$ in a uniformly rotating flow.

When the gap is wide ($A \lesssim 2$ in (5.2)), R_m and ζ may vary considerably across the gap, and it is useful to define mean values of these dimensionless parameters. Following Paper I, we introduce $\bar{\Omega} \equiv \sqrt{\Omega_1\Omega_2}$ and

$$\bar{R}_m \equiv \frac{\bar{\Omega}}{\eta K^2}, \quad \bar{\zeta} \equiv \frac{2(r_2^2\Omega_2 - r_1^2\Omega_1)}{(r_2^2 - r_1^2)\bar{\Omega}}. \tag{5.8}$$

The locus of marginal stability is actually a hypersurface in the space $(P_m, A, \epsilon, \bar{\zeta}, S, \bar{R}_m)$. The curves in figure 1 are cuts through this locus at constant values of the first four parameters: $P_m = 0$ and $P_m = 1.6 \times 10^{-6}$; $A = \epsilon = 1$; and two positive values of $\bar{\zeta}$ as indicated. The curves are drawn in physical units for the density and diffusivity of gallium.
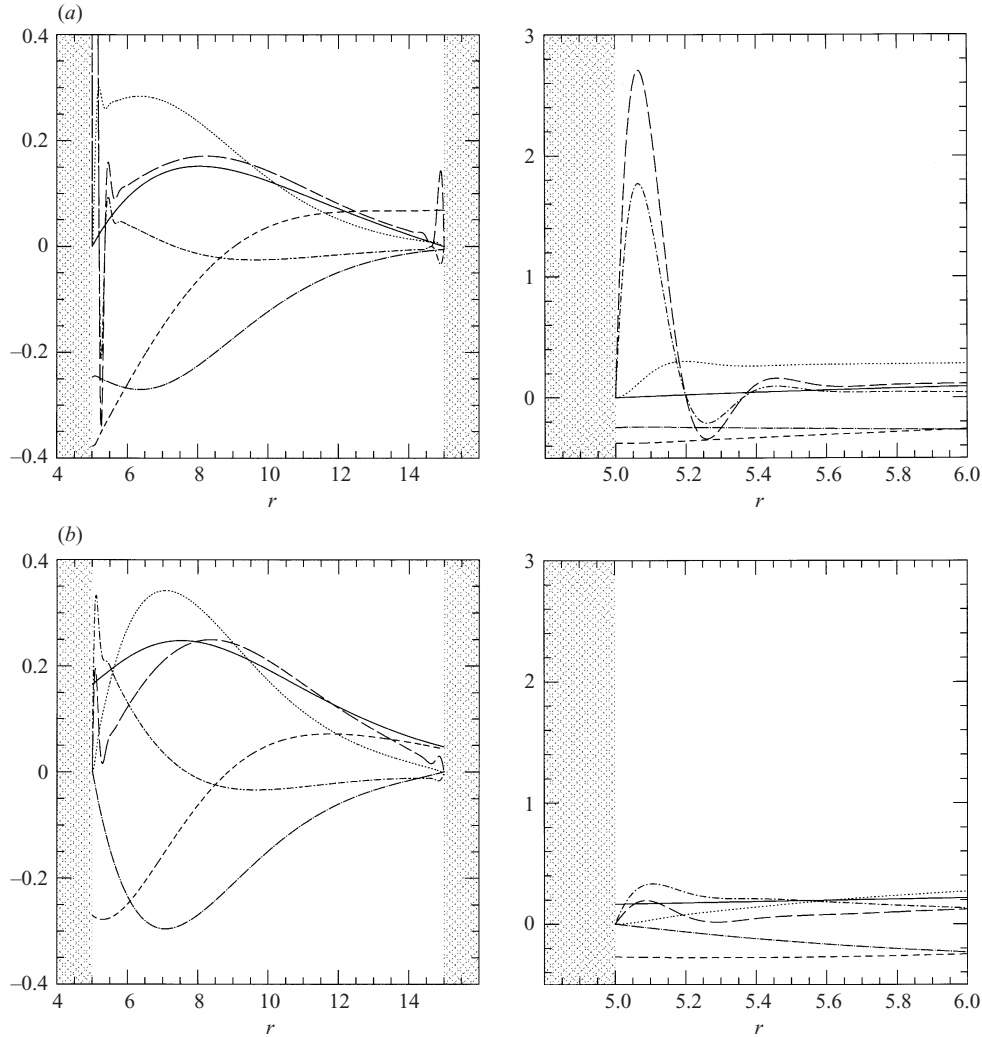
FIGURE 2. (*a*) Marginal eigenmode with conducting boundaries, for $B = 3\,\mathrm{kG}$, $\Omega_1 = 314$, $\Omega_2 = 37.9\,\mathrm{rad\,s^{-1}}$ and $\bar{\zeta} = 0.0632$. Left-hand panel: full gap. Right-hand panel: expanded view near the inner cylinder. Solid curves: β_r; short-dashed: β_z; dot-long-dashed: $\beta_\theta \times 5$; dotted: $\varphi_r \times 1/3$; long-dashed: φ_θ; dot-short-dashed: $\varphi_z \times 0.07$. (*b*) As (*a*) but for insulating boundaries and $\Omega_1 = 284$, $\Omega_2 = 34.4\,\mathrm{rad\,s^{-1}}$, $\bar{\zeta} = 0.0632$.

The inviscid results shown in this figure were calculated by an independent numerical method based on equation (4.1), which we have unpacked into a pair of second-order equations (using (3.3) with $s, v \to 0$):

$$\mathrm{D}_k \beta_r = \frac{r\omega_A^2}{\eta(r^2\Omega)'}\beta_\theta = K^2 \frac{S^2}{\zeta R_m}\beta_\theta, \tag{5.9}$$

$$\mathrm{D}_k \beta_\theta = \frac{\omega_A^4 r}{2\Omega(r^2\Omega)'\eta^2 k^2}\beta_\theta - \frac{r\Omega'}{\eta}\beta_r = K^2 \left[\frac{(1+\epsilon^2)S^4}{2\zeta R_m^2}\beta_\theta + (2-\zeta)R_m\beta_r\right], \tag{5.10}$$

together with the magnetic boundary conditions (2.7) or (2.8). Because of the large
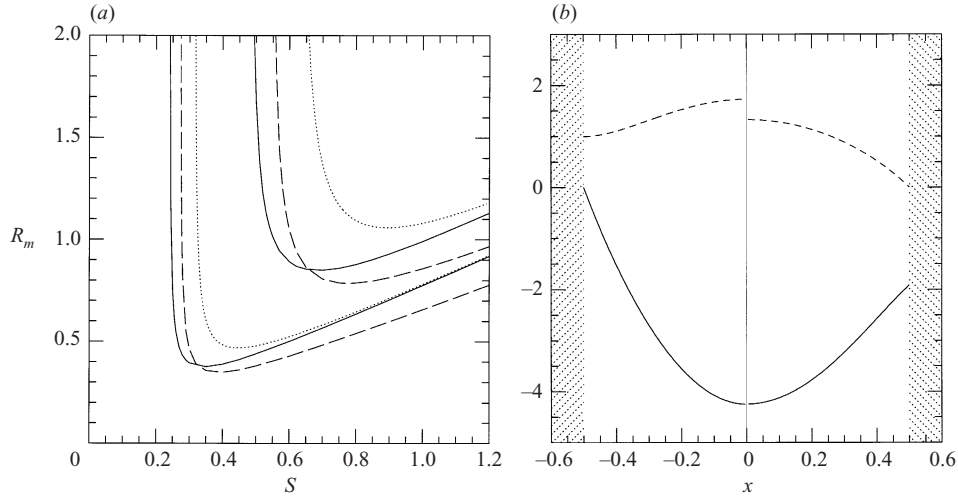
FIGURE 3. Narrow-gap modes for $P_m = 0$ and $\epsilon = 1$. (*a*) Curves of marginal stability for $\zeta = 2/11$ (lower curves) and $\zeta = 4/7$ (upper). Solid line for conducting walls, dashed for insulating, and dotted for local approximation (5.11). (*b*) Narrow-gap eigenfunctions β_r (solid curves) and β_θ (dashed), for $\zeta = 2/11$ and $S = 0.4$. Since eigenfunctions are symmetric about the centre of the gap ($x = 0$), only half of each is shown: conducting on the left, insulating on the right.

magnetic diffusivity, the magnetic variables are very well-behaved, so that this fourth-order system can be solved efficiently by a shooting method.

Comparing figures 2(*a*) and 2(*b*), one sees that viscosity is more important for conducting boundary conditions than for insulating ones. In the conducting case, φ_r and β_θ are nearly proportional to one another throughout most of the flow (figure 2*a*). This follows from equation (2.3) in the limit $s, v \to 0$, as we discussed in §4. Since the radial velocity perturbation ($\propto \varphi_r$) must vanish at the wall but the azimuthal magnetic perturbation ($\propto \beta_\theta$) does not, there is a thin boundary layer in which viscous stress balances the azimuthal magnetic force. The right-hand panel shows that the boundary layer is resolved well by these calculations, which use 4000 grid points uniformly spaced in $\ln r$ across the gap. At an insulating boundary, on the other hand, β_θ vanishes with φ_r, and this leads to a much less dramatic viscous layer (figure 2*b*). The characteristic boundary-layer thickness (4.5) is $\delta \approx 0.054$ cm at $r = r_1$ in both of these cases; the microscopic roots of (4.7) are predicted to have a damped oscillation with wavelength $(4\pi/\sqrt{3})\delta \approx 0.39$ cm, clearly in agreement with the right-hand panel of figure 2(*a*).

The narrow-gap limit $A \to \infty$ is experimentally impractical but theoretically important. Figure 3 shows eigenfunctions and curves of marginal stability in this limit. Because of the boundary conditions, the eigenfunctions cannot be sinusoidal in r or $x \equiv (r - r_1)/d$, even though the equations of motion have elementary solutions of this form. The fourth-order inviscid system (5.9) and (5.10) has four roots for the radial wavenumber (or two if sign is ignored) at given parameters $(\epsilon, S, R_m, \zeta)$ of the equilibrium, which are constant across the gap. (Note K is not an independent parameter, since $Kd = \sqrt{\epsilon^2 + 1}$.) The solutions satisfying the boundary conditions are linear combinations of four complex exponentials, each containing one of these wavenumbers, and the parameters $(\epsilon, S, R_m, \zeta)$ must satisfy one constraint in order that a solution exist. If, however, one simply sets $k_r = \pi/d$ in the hope of obtaining an approximate constraint, then $D_k \to -K^2$ and equations (5.9) and (5.10) or (4.1)

	$\Omega_1 = 413.6$, $\Omega_2 = 50\,\mathrm{rad\,s^{-1}}$				$\Omega_1 = 377.0$, $\Omega_2 = 40.84\,\mathrm{rad\,s^{-1}}$		
B_z [G]	Conducting [s^{-1}]	Insulating [s^{-1}]	Local [s^{-1}]	B_z [G]	Conducting [s^{-1}]	Insulating [s^{-1}]	Local [s^{-1}]
1893	0.00	—	—	0	16.07	16.07	17.11
2135	5.35	0.00	—	500	17.46	17.00	17.98
2500	9.46	6.46	6.55	1000	20.10	19.04	19.85
3000	11.50	10.83	10.48	1500	22.23	21.07	21.58
3500	10.96	12.66	11.36	2000	23.20	22.50	22.49
4000	8.42	12.84	9.99	3000	21.13	22.83	20.78
4500	4.16	11.78	6.63	4000	14.04	19.82	13.50
4868	0.00	10.38	2.91	5000	4.219	14.38	—
5500	—	7.10	—	5500	1.438	11.22	—
6000	—	3.97	—	6000	—	8.093	—
6588	—	0.00	—	6500	—	5.261	—
				7000	—	2.987	—
				8000	—	0.8246	—
				9000	—	0.4272	—
				10000	—	0.2131	—
				11000	—	3.614e-2	—
				11220	—	0	—

TABLE 1. Growth rates in gallium.

would yield

$$R_m^2 = S^2 \frac{1 + \epsilon^2}{2(2 - \zeta - \zeta S^{-2})}. \tag{5.11}$$

This corresponds to the dispersion relation for marginal modes obtained in Paper I from a local WKB analysis with a ratio ϵ of vertical to horizontal wavelength. Evidently there exists a minimum Lundquist number for instability,

$$S_{\min} = \sqrt{\frac{\zeta}{2 - \zeta}}, \tag{5.12}$$

and in the opposite limit of large S,

$$\frac{R_m}{S} = \frac{\Omega}{k V_A} \approx \sqrt{\frac{1 + \epsilon^2}{2(2 - \zeta)}}. \tag{5.13}$$

Figure 3 shows that the predictions (5.11)–(5.13) are qualitatively correct.

Numerical growth rates are given in table 1 for two representative angular-velocity profiles, both with $r_2 = 3r_1 = 15\,\mathrm{cm}$, $h = 10\,\mathrm{cm}$, and the material properties of gallium. The first case has $\bar{\zeta} = 0.063$ and hence is Rayleigh-stable. The second has $\bar{\zeta} = -0.019$, so that the Rayleigh instability occurs at zero field strength. Growth rates are shown for conducting and insulating radial boundary conditions. Larger fields are required to initiate and to quench MRI with insulating boundaries than with conducting ones, presumably because perturbed lines of force expand past insulating walls into a volume slightly larger than the Couette flow itself. The final column of this table shows growth rates computed from the algebraic local dispersion relation given in Paper I. Once again the WKB analysis predicts the global growth rates remarkably well, even though the wavelengths involved are actually larger than the
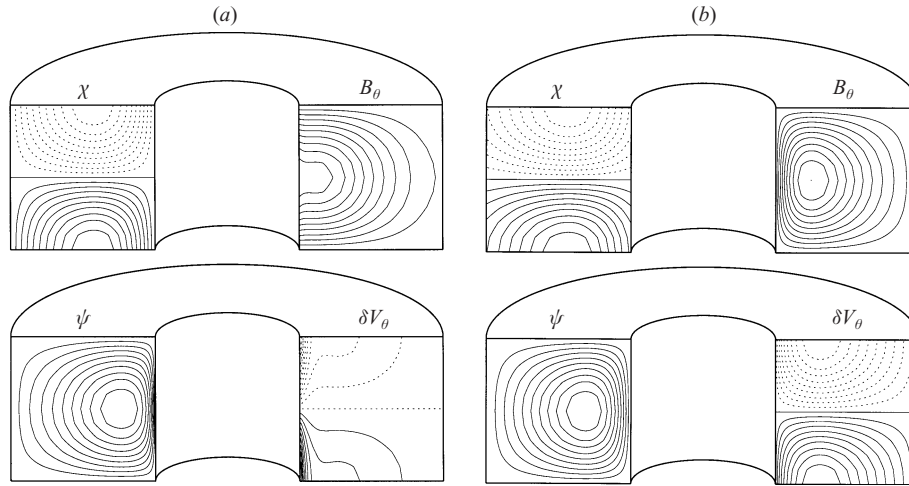
FIGURE 4. Visualizations of the MRI eigenmodes for the Rayleigh-stable cases from table 1 at $B_{z,0} = 3 \, \mathrm{kG}$: (*a*) conducting boundaries, (*b*) insulating. Solid and dotted lines indicate positive and negative values, respectively. See equation (5.14) for definitions of flux and stream functions χ, ψ.
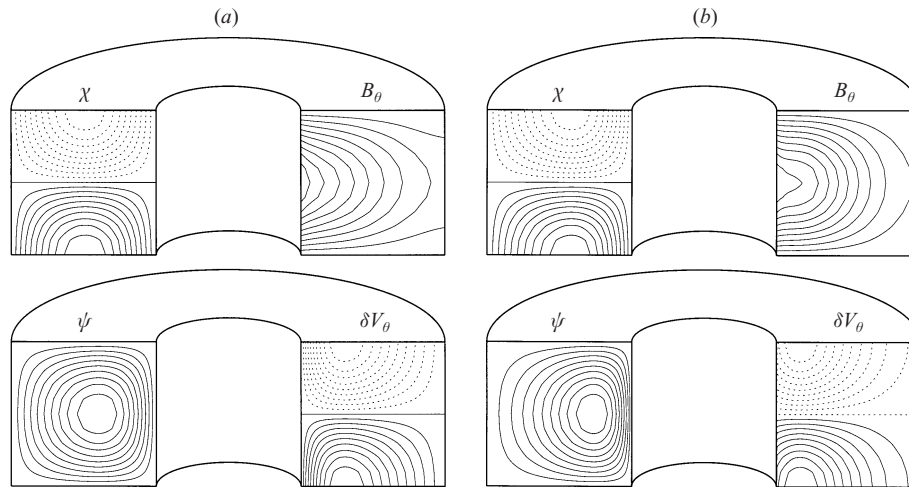

FIGURE 5. Rayleigh-unstable cases from table 1 at of $B_{z,0} = 0 \, \mathrm{kG}$ (*a*) and $3 \, \mathrm{kG}$ (*b*), both with conducting boundaries.

gap width, and the angular velocity and shear rate vary by a factor ≈ 9 across the gap.

Figures 4 and 5 show two-dimensional cross-sections of selected modes from table 1. The flux and stream functions are related to the poloidal perturbations by

$$\frac{\delta \boldsymbol{B}_P}{(4\pi\rho)^{1/2}} = \nabla\theta \times \nabla\chi, \quad \delta\boldsymbol{v}_P = \nabla\theta \times \nabla\psi. \tag{5.14}$$

In all cases, the poloidal velocity field consists of a single roll. The effect of the choice of boundary conditions is seen most clearly in the azimuthal perturbations. In figure 4(*a*) and figure 5(*b*), it looks as though δv_θ does not vanish at the inner boundary; in fact it does vanish, but the viscous boundary layer is too small to be resolved by these plots. Figure 5(*a*) does not show this behaviour because the magnetic

forces are absent; this mode is a classical hydromagnetic centrifugal instability. A boundary layer of the ordinary nonmagnetic variety occurs in δv_z. The corresponding magnetized case shown in figure 5(*b*) has a magnetically driven boundary layer similar to that of the Rayleigh-stable flows.

6. Summary and discussion

We have presented a global linear stability analysis for magnetized Couette flow, including the dissipative effects of viscosity and resistivity, in regimes where magneto-rotational instability (MRI) is possible. In view of the properties of liquid metals, and for plausible experimental lengthscales, resistivity is the main obstacle that must be overcome to demonstrate MRI. Previous theoretical studies of magnetized Couette flow have focused on the problem of suppressing Rayleigh instability with a magnetic field, and they have simplified the induction equations so as to reduce the number of radial and time derivatives in the problem. Such approximations may be adequate for the regime of interest to those studies, but not if one is interested in MRI. Therefore we have worked with the full induction equations.

Particular attention has been given to marginal stability. All of our numerical evidence indicates that exchange of stability occurs at vanishing complex growth rates; we have not encountered any overstable modes. In the inviscid limit of marginal stability, the number of radial derivatives reduces from ten to four, but the velocity perturbations become singular at conducting boundaries. The dominant singularity arises from an unbalanced tangential magnetic force, not from the usual pressure and inertial effects that cause boundary layers in unmagnetized fluids. Despite these complications, the inviscid approximation predicts the locus of marginal stability reasonably well for liquid metals.

Solving the linearized initial-value problem by finite differences, we have calculated growth rates and stability boundaries for a liquid metal approximating gallium in an experimentally plausible geometry. For easier comparison with other theoretical work, we have also made calculations in the narrow-gap limit and expressed our results in the dimensionless coordinates of Lundquist number and magnetic Reynolds number.

Remarkably, the growth rates are predicted reasonably well by a simple WKB approximation even though the WKB modes do not satisfy the boundary conditions and have a radial wavelength twice the gap width, and even when the rotation rate varies by an order of magnitude across the gap. We conclude from this that the algebraic WKB dispersion relation can be used for preliminary experimental design, at least for gaps no wider than considered here ($r_2 : r_1 = 3 : 1$).

There are good reasons to attempt an MRI experiment. First, one can hardly exaggerate the importance of this instability: few or no plausible alternative explanations exist for the dissipation of orbital energy in accretion disks, which are fundamental to so many of the most energetic sources known in the universe. Yet all present knowledge of the instability is purely theoretical, based as it is on linear analysis and computer simulation; the constraints provided by astronomical observations are very indirect. It is prudent to put these theories to a laboratory test.

Secondly, computer speed limits the range of spatial scales that can be modelled in the simulations. Barring unforseen algorithmic breakthroughs, the smallest resolvable scale in a three-dimensional simulation improves only as the fourth root of the rate of arithmetic operations. Here it must be acknowledged that the large magnetic diffusivity of liquid metals severely limits the number of degrees of freedom in the magnetic field that can be excited. The simulations are well ahead of any forseeable

experiment in this respect. In fact, simulations indicate that magnetic Reynolds numbers and Lundquist numbers at least 100 times larger than the minimum necessary for linear instability are required for dynamo action in the absence of an externally imposed field parallel to the rotation axis (Fleming *et al.* 2000). On the other hand, the viscous Reynolds number of such an experiment would be $Re = P_m^{-1} R_m \gtrsim 10^6$, a value still out of reach of direct numerical simulations. Also, small R_m need not restrict the experiment to linear behaviours. In the local disk simulations of Fleming *et al.* (2000) at about twice the minimum R_m for linear MRI, a violently fluctuating nonlinear state was reached in which the time-averaged magnetic energy was about 25 times larger than that of the externally imposed field. Similar calculations and results have recently been reported by Sano & Inutsuka (2001).

Although large R_m is the rule in astrophysics, the dimensionless parameters of some systems may be similar to those of our proposed experiment, namely R_m and S of order unity, Re very large, and an externally imposed field. Such systems include the inner parts of relatively cool disks (protostellar disks and quiescent cataclysmic variables, for example) around stars with their own magnetic moments (Gammie 1996; Gammie & Menou 1998).

Lastly, relatively little laboratory MHD work has been done in which the inertia of the fluid is important (large plasma β). The experimental field appears somewhat underdeveloped when measured against its potential importance to geophysics and astrophysics. Because it promises to be achievable at fairly modest cost in a classic experimental framework (Couette flow), MRI is a good place to start.

Appendix. Derivation of linearized equations

For completeness, equations (2.2)–(2.6) are derived here, although much the same derivation can be found in Chandrasekhar (1961). The equations of incompressible MHD are

$$\dot{\boldsymbol{B}} + \boldsymbol{v} \cdot \nabla \boldsymbol{B} - \boldsymbol{B} \cdot \nabla \boldsymbol{v} = \eta \nabla^2 \boldsymbol{B}, \quad \nabla \cdot \boldsymbol{B} = 0,$$

$$\dot{\boldsymbol{v}} + \boldsymbol{v} \cdot \nabla \boldsymbol{v} + \rho^{-1} \nabla P - \frac{\boldsymbol{B} \cdot \nabla \boldsymbol{B}}{4\pi\rho} = \nu \nabla^2 \boldsymbol{v}, \quad \nabla \cdot \boldsymbol{v} = 0,$$

in which $P \equiv p + \boldsymbol{B}^2/8\pi$ is the hydrodynamic plus magnetic pressure. In cylindrical coordinates, near an equilibrium $\boldsymbol{B}_0 = B\boldsymbol{e}_z = \text{constant}$ and $\boldsymbol{v}_0 = r\Omega(r)\boldsymbol{e}_\theta$, linearized axisymmetric perturbations $\delta\boldsymbol{v}$ and $\delta\boldsymbol{B}$ satisfy

$$\delta\dot{B}_r - B\partial_z \delta v_r = \eta(\partial_r \partial_r^\dagger + \partial_z^2)\delta B_r, \tag{A 1}$$

$$\delta\dot{B}_\theta - B\partial_z \delta v_\theta - \delta B_r r \partial_r \Omega = \eta(\partial_r \partial_r^\dagger + \partial_z^2)\delta B_\theta, \tag{A 2}$$

$$\delta\dot{v}_r - 2\Omega\delta v_\theta + \partial_r \frac{\delta P}{\rho} - \frac{B}{4\pi\rho}\partial_z \delta B_r = \nu(\partial_r \partial_r^\dagger + \partial_z^2)\delta v_r, \tag{A 3}$$

$$\delta\dot{v}_\theta + \delta v_r \partial_r^\dagger(r\Omega) - \frac{B}{4\pi\rho}\partial_z \delta B_\theta = \nu(\partial_r \partial_r^\dagger + \partial_z^2)\delta v_\theta, \tag{A 4}$$

$$\delta\dot{v}_z + \partial_z \frac{\delta P}{\rho} - \frac{B}{4\pi\rho}\partial_z \delta B_z = \nu(\partial_r^\dagger \partial_r + \partial_z^2)\delta v_z, \tag{A 5}$$

$$\partial_r^\dagger \delta B_r + \partial_z \delta B_z = 0, \tag{A 6}$$

$$\partial_r^\dagger \delta v_r + \partial_z \delta v_z = 0, \tag{A 7}$$

in which the dot denotes $\partial/\partial t$, and other recurring operators are

$$\partial_z \equiv \frac{\partial}{\partial z}, \quad \partial_r \equiv \frac{\partial}{\partial r}, \quad \partial_r^\dagger \equiv \frac{\partial}{\partial r} + \frac{1}{r}.$$

Equations (A 3) and (A 5) presume that ρ, like η and v, is spatially constant. Applying $\partial_r^\dagger$ to equation (A 3) and ∂_z to equation (A 5) and summing the results, one finds that

$$(\partial_r^\dagger \partial_r + \partial_z^2)\frac{\delta P}{\rho} = \partial_r^\dagger (2\Omega \delta v_\theta),$$

in view of equations (A 6) and (A 7). With another application of ∂_r, this becomes

$$(\partial_r \partial_r^\dagger + \partial_z^2)\Pi = \partial_z^2 (2\Omega \delta v_\theta), \quad \text{where} \quad \Pi \equiv 2\Omega \delta v_\theta - \partial_r \frac{\delta P}{\rho}, \tag{A 8}$$

so that the radial Euler equation (A 3) can be stated as

$$\delta \dot{v}_r - \Pi - \frac{B}{4\pi\rho}\partial_z \delta B_r = v(\partial_r \partial_r^\dagger + \partial_z^2)\delta v_r. \tag{A 9}$$

With the z dependences given by equation (2.1) for the linearized quantities, equations (A 2), (A 4), (A 1), (A 9) and (A 8) reduce to equations (2.2), (2.3), (2.4), (2.5) and (2.6), respectively.

REFERENCES

ARLT, R. & RÜDIGER, G. 2001 Global accretion disk simulations of magneto-rotational instability. *Astron. Astrophys.* **374**, 1035–1048.

ARMITAGE, P. J. 1998 Turbulence and angular momentum transport in global accretion disk simulation. *Astrophys. J.* **501**, L189–L192.

BALBUS, S. A. & HAWLEY, J. F. 1991 A powerful local shear instability in weakly magnetized disks. I. Linear analysis. *Astrophys. J.* **376**, 214–233.

BALBUS, S. A. & HAWLEY, J. F. 1992 A powerful local shear instability in weakly magnetized disks. IV. Nonaxisymmetric perturbations. *Astrophys. J.* **400**, 610–621.

BALBUS, S. A. & HAWLEY, J. F. 1998 Instability, turbulence, and enhanced transport in accretion disks. *Rev. Mod. Phys.* **70**, 1–53.

BRAHME, A. 1970 On the hydromagnetic stability of a nonuniformly rotating fluid. *Physica Scripta* **2**, 108–112.

BRANDENBURG, A., NORDLUND, A., STEIN, R. F. & TORKELSSON, U. 1995 Dynamo-generated turbulence and large-scale magnetic fields in a keplerian shear flow. *Astrophys. J.* **446**, 741–754.

CHANDRASEKHAR, S. 1960 The stability of non-dissipative Couette flow in hydromagnetics. *Proc. Natl Acad. Sci.* **46**, 253–257.

CHANDRASEKHAR, S. 1961 *Hydrodynamic and Hydromagnetic Stability*. Oxford University Press.

CHANG, T. S. & SARTORY, W. K. 1967 On the onset of instability by oscillatory modes in hydromagnetic Couette flow. *Proc. R. Soc. Lond.* A **301**, 451–474.

CHEN, C.-K. & CHANG, M. H. 1998 Stability of hydromagnetic dissipative Couette flow with non-axisymmetric disturbance. *J. Fluid Mech.* **366**, 135–158.

CURRY, C. & PUDRITZ, R. E. 1995 On the global stability of magnetized accretion disks. II. Vertical and azimuthal magnetic fields. *Astrophys. J.* **453**, 697–714.

DONNELLY, R. J. & CALDWELL, D. R. 1964 Experiments on the stability of hydromagnetic Couette flow. *J. Fluid Mech.* **19**, 257–263.

DONNELLY, R. J. & OZIMA, M. 1960 Hydromagnetic stability of flow between rotating cylinders. *Phys. Rev. Lett.* **4**, 497–498.

Donnelly, R. J. & Ozima, M. 1962 Experiments on the stability of flow between rotating cylinders in the presence of magnetic field. *Proc. R. Soc. Lond.* A **266**, 272–286.

Fleming, T. P., Stone, J. M. & Hawley, J. F. 2000 The effect of resistivity on the nonlinear stage of the magnetorotational instability in accretion disks. *Astrophys. J.* **530**, 464–477.

Gammie, C. F. 1996 Layered accretion in T Tauri disks. *Astrophys. J.* **457**, 355–362.

Gammie, C. F. & Balbus, S. A. 1994 Quasi-global linear analysis of a magnetized disc. *Mon. Not. R. Astron. Soc.* **270**, 138–152.

Gammie, C. F. & Menou, K. 1998 On the origin of episodic accretion in dwarf novae. *Astrophys. J.* **492**, L75–L78.

Hassard, B. D., Chang, T. S. & Ludford, G. S. S. 1972 An exact solution in the stability of m.h.d. Couette flow. *Proc. R. Soc. Lond.* A **327**, 269–278.

Hawley, J. F. 2001 Global magnetohydrodynamic simulations of cylindrical keplerian disks. *Astrophys. J.* **554**, 534–547.

Hawley, J. F., Balbus, S. A. & Stone, J. M. 2001 A magnetohydrodynamic nonradiative accretion flow in three dimensions. *Astrophys. J.* **554**, L49–L52.

Hawley, J. F., Gammie, C. F. & Balbus, S. A. 1995 Local three-dimensional magnetohydrodynamic simulations of accretion disks. *Astrophys. J.* **440**, 742–763.

Hawley, J. F., Gammie, C. F. & Balbus, S. A. 1996 Local three-dimensional simulations of an accretion disk hydromagnetic dynamo. *Astrophys. J.* **464**, 690–703.

Hawley, J. F. & Krolik, J. H. 2001 Global MHD simulation of the inner accretion disk in a pseudo-newtonian potential. *Astrophys. J.* **548**, 348–367.

Ji, H., Goodman, J. & Kageyama, A. 2001 Magnetorotational instability in a rotating liquid metal annulus. *Mon. Not. R. Astron. Soc.* **325**, L1–L5 (referred to herein as Paper I).

Knobloch, E. 1992 On the stability of magnetized accretion discs. *Mon. Not. R. Astron. Soc.* **255**, 25P–28P.

Machida, M., Hayashi, M. R. & Matsumoto, R. 2000 Global simulations of differentially rotating magnetized disks: formation of low-β; filaments and structured coronae. *Astrophys. J.* **532**, L67–L70.

Matsumoto, R., Uchida, Y., Hirose, S., Shibata, K., Hayashi, M. R., Ferrari, A., Bodo, G. & Norman, C. 1996 Radio jets and the formation of active galaxies: accretion avalanches on the torus by the effect of a large-scale magnetic field. *Astrophys. J.* **461**, 115–126.

Ogilvie, G. I. & Pringle, J. E. 1996 The non-axisymmetric instability of a cylindrical shear flow containing an azimuthal magnetic field. *Mon. Not. R. Astron. Soc.* **279**, 152–164.

Roberts, P. H. 1967 *An Introduction to Magnetohydrodynamics*. Longmans, Green & Co. Ltd.

Sano, T. & Inutsuka, S.-I. 2001 Saturation and thermalization of the magnetorotational instability: recurrent channel flows and reconnections. *Astrophys. J.* **561**, L179–L182.

Soundalgekar, V. M., Ali, M. A. & Takhar, H. S. 1994 Hydromagnetic stability of dissipative Couette flow: wide-gap problem. *Intl J. Energy Res.* **18**, 689–695.

Stone, J. M. & Norman, M. L. 1994 Numerical simulations of magnetic accretion disks. *Astrophys. J.* **433**, 746–756.

Takhar, H. S., Ali, M. A. & Soundalgekar, V. M. 1989 Stability of MHD Couette flow in a narrow gap annulus. *Appl. Sci. Res.* **46**, 1–24.

Terquem, C. & Papaloizou, J. C. B. 1996 On the stability of an accretion disc containing a toroidal magnetic field. *Mon. Not. R. Astron. Soc.* **279**, 767–784.

Velikhov, E. P. 1959 Stability of an ideally conducting liquid flowing between cylinders rotating in a magnetic field. *Sov. Phys. JETP* **36** (9), 995–998.

Vislovich, A. N., Novikov, V. A. & Sinitsyn, V. A. 1986 Influence of a magnetic field on the Taylor instability in magnetic fluids. *J. Appl. Mech. Tech. Phys.* **27** (1), 72–78.